

Stages of structural transformation in iron thin film growth on copper (100)

J. Giergiel ^{*,1}, J. Kirschner, J. Landgraf, J. Shen, J. Woltersdorf

Max-Planck-Institut für Mikrostrukturphysik, Weinberg 2, D-06120 Halle, Germany

(Received 11 August 1993; accepted for publication 1 December 1993)

Abstract

We report on an attempt for a complete qualitative investigation of $\gamma \rightarrow \alpha$ phase transformation in iron films grown at room temperature on Cu(100). To this end we characterize the surface morphology across the full transformation range using a special scanning tunneling microscope that allows imaging one particular area of the sample as it undergoes the growth induced transformation. We report for the first time, that the system is unstable toward a structural rearrangement at coverages as low as 4.6 ML, that it develops a very characteristic network of surface features and we will describe these features and their evolution in detail. The structural transformation is initiated by formation of dislocation-like thin elongated ridges which later transform into a very complicated system of bcc precipitates. Several paths of these transformations are identified. Their multiplicity reflects the complexity of processes that drive this transformation. A brief description of driving forces, a possible transformation mechanism and a correlation with magnetic properties will be given.

1. Introduction

Bulk iron has four allotropic forms, known as α , β , γ and δ , with transition points at 770, 928 and 1530°C [1]. The α form is magnetic, but when transformed into the β form, the magnetism disappears although the bcc lattice remains unchanged. The high temperature γ phase has an fcc structure [2], which cannot be retained on quenching in pure bulk iron. However, numerous studies have shown that the fcc γ -phase can be stabilized at room temperature in ultrathin films

of iron grown epitaxially on the Cu(100) surfaces. Such films were predicted [3–5] and shown [6,7] to have striking magnetic properties that depend dramatically on their thickness. The origin of this behavior is clearly connected with the reduced dimensionality of the magnetic system, but to a large measure must also be influenced by morphology and structural properties of the film. Extensive experimental investigations of this pseudo-epitaxial system reveal a very complicated growth mode [8–11].

A glimpse at the overall behavior of the system can be obtained from any of the area-integrating methods: medium-energy electron diffraction (MEED) [12], reflection high-energy electron diffraction (RHEED) [13], helium beam scattering [14,15] and low-energy ion-scattering [11].

* Corresponding author.

¹ On leave of absence from Department of Physics, University of California, Irvine, CA, 92717, USA.

They all agree that the growth of iron on Cu(100) can be separated into three distinct regions.

At low coverages (region I) room temperature (RT) deposited iron films show Volmer–Weber (VW) like growth mode as expected from the balance of surface and interface free energies. The characteristic features of this stage are high nucleation density and multilayer island structures. The issue of possible intermixing between copper and iron during the initial stages of growth has been discussed by several groups [11,16,17] but appears to be still unresolved. Then, the growth mode gradually switches to Frank–Van der Merwe (FV) mode as inferred from the appearance of regular oscillations in MEED intensities at around 4–5 ML thick iron film.

At higher coverages (region II) the system seems to grow epitaxially. According to one I/V LEED structure determination [10], the in-plane lattice constant is that of the underlying Cu(100) while the interplanar spacing is slightly contracted resulting in a face centered tetragonal (fct) unit cell. Real space data obtained by scanning tunneling microscopy (STM) confirm MEED results by showing what essentially is a layer by layer growth morphology [17].

Above some critical thickness the film shows signs of disorder as indicated by gradual decrease in MEED intensity and disappearance of MEED [18] oscillations and by more recent real space data [16,18,19]. This is region III. The exact starting point of region III is not well known, it varies from 10 to 21 ML depending on the source of data and on the resolving power of the experimental technique used to detect it. The characteristic feature of the iron film in this region is the existence of bcc precipitates as recently established by Wuttig et al. [18]. In another recent work (Chambliss et al. [16]), phase III has been identified as a parent-product phase mixture resulting from a martensitic transformation from fcc to bcc iron. Several other aspects of this transformation have been recently investigated with X-ray photoelectron forward scattering [20].

The work reported here extends on Wuttig and Chambliss results by carefully following this phase transformation across its full range and by describing in greater detail the evolution of sur-

face relief on one particular surface area. We restrict our investigation to effects of film thickness only; the thermal treatment (annealing, cooling) was intentionally avoided as it complicates the already very complicated system. We report for the first time, that the system is unstable toward a structural rearrangement at coverages as low as 4.6 ML (i.e. at the beginning of phase II) and that it develops a very characteristic two-dimensional network of surface features. We will describe in detail these features and their evolution. The structural transformation is initiated by formation of dislocation-like thin elongated ridges which later transform into a very complicated system of bcc precipitates. Several paths of these transformations are identified. Their multiplicity reflects the complexity of processes that drive this transformation. A brief description of driving forces, a possible transformation mechanism and the correlation with magnetic properties will be given.

The paper is organized as follows: in the next section we discuss general aspects of the $\gamma \rightarrow \alpha$ phase transformation in iron with special emphasis on thin film growth. Then we give a brief description of experimental procedures followed by a detailed presentation of experimental results and their discussion.

2. Aspects of $\gamma \rightarrow \alpha$ thin film transformations

It has been recently realized [18,21] that the disorder observed in phase III must be connected with the fact that the iron film in the γ -Fe/Cu(100) system is inherently unstable for two reasons. It is strained because of the -1.1% lattice mismatch between fcc iron and fcc copper. In case of continued pseudomorphic growth the energy associated with this mismatch increases with increasing film thickness and can be relieved at a certain critical thickness by a dislocation network. The second destabilizing factor is a large difference in the total energy of the two crystallographic forms of iron (on the order of 0.018 eV/atom [22]). This difference is responsible for the bcc form being stable for up to 928°C and for

the fact that the fcc phase cannot be retained on quenching in pure iron.

At a certain critical stage of film growth the system of γ -Fe layers on Cu(100) must, therefore, become unstable with respect to a spontaneous transformation into the bcc form according to basic thermodynamical considerations. As discussed before, such a transformation has, indeed, been observed [16,18]. However, the exact nature of this transformation and the mechanisms of the lattice rearrangements are unknown.

As in iron–carbon alloys, the $\gamma \rightarrow \alpha$ transformation of *pure* iron can also proceed via a diffusionless mechanism of lattice rearrangement denoted as martensitic. The atoms forming the lattice of γ -iron shift more or less abruptly over certain distances along given directions in order to occupy sites corresponding to the lattice of α -iron. At least at high cooling rates the martensitic nature of the $\gamma \rightarrow \alpha$ transformation in pure iron has already been demonstrated in the sixties [23]. Moreover, the formation of Widmannstätten ferrite [24] was also shown to be martensitic [25].

Various limiting conditions such as cooling parameters, state of stress and nucleation conditions will decide if (a) the process of atomic rearrangement is martensitic in a strong sense, i.e. acting through a pure collective shear displacement maintaining the atomic neighborhood, or if (b) the process of rearrangement is supported by a thermally activated exchange of atoms along the interface between α - and γ -phases.

In carbon-containing systems the transformation process may lead to the martensite (Fe–C) phase depending on cooling rate and mobility of the C-atoms. The evolution of this transformation process is influenced by the superimposed tetragonal strains due to incorporation of carbon atoms which are controlling the c/a ratio.

It is well known that this transformation is crystallographically a rather complex phenomenon since several habit planes are possible with mostly irrational indices, preferentially, however, near $\{111\}\gamma$, $\{112\}\gamma$, $\{225\}\gamma$, $\{259\}\gamma$, $\{3,10,15\}\gamma$. Besides, there are also several orientation relationships between the α - and the γ -phases depending on the influence of applied mechanical stress and the micro-chemistry [26].

That means that structurally, the martensitic $\gamma \rightarrow \alpha$ transition is not unambiguously pre-determined. Thus, special growth conditions, boundary conditions and structural defects may imply that several modifications of the atomic rearrangement are compatible simultaneously and can replace each other.

Even slight changes in the defect concentration, particularly of carbon, may drastically vary the governing parameters of the redistribution. These are the stacking fault energies, the martensitic starting temperature M_s , the critical shear stresses for gliding and twin nucleation as well as the elastic constants of the α - and γ -phases.

A further influencing of the transformation mechanisms will occur in the case of ultrathin film growth if interface and surface effects are superimposed and the growth morphology is determined by effects of pseudomorphism, misfit strain and generation of misfit dislocations [27], which can act as nucleation centers for the transformation. A characteristic feature of the formation of martensite (in the sense of the product phase of martensitic transformation) is the occurrence of a surface relief [28] for reducing the overall shear, the crystallography of which can give information concerning the details of the phase transition. The early work by Jesser and Matthews [29,30] and by Olsen and Jesser [31,32] on iron films grown under UHV conditions and later transferred in air to an electron microscope can serve as a useful guide despite the fact that the contamination level of the copper substrate and the iron film was not determined. Nevertheless, evidence was found for the formation of α iron nuclei in the thicker parts of the deposits and some possibilities of orientation relationships between the γ and α phases were suggested. In the recent UHV work of Wuttig et al. [18] and Chambliss et al. [16] the coexistence of γ and α phases was confirmed and the crystallographical aspects of the transformation were considered. Several characteristic features of structural rearrangement were reported: the appearance of protruding islands on a 10 ML thick film, metastability upon cooling or sputtering, the effects of annealing on morphology and transformation phenomena [18], and, additionally, the existence of

narrow elongated streaks and the twinning of grain boundaries [16].

3. Experimental

3.1. Surface preparation and film growth

The copper substrate cut to within 0.5° of the (100) plane was prepared by low energy ion-sputtering (Ne, 300 eV) at 870 K followed by controlled linear cooling to 790 K and natural cooling to room temperature (450 K in 5 min, RT in ~ 2 h). The resultant surface was contamination free within the detection limits of the CMA based Auger spectrometer (0.1 at% for most elements), and had large atomically smooth areas of typical linear dimensions on the order of several hundreds of a nm. Fig. 1a shows a typical topography of a clean copper surface. Note the surface fault line terminating at two screw dislocations (*along the bottom of the image*). A surface area with such a feature was intentionally chosen to facilitate the subsequent retrieval of the same

location on the surface and as a special site for determination of effects of dislocations on film morphology and subsequent transformation behavior.

The iron films were grown at room temperature (300 ± 5 K) with evaporation rates of less than 0.3 ML/min. The base pressure of the chamber was 9×10^{-9} Pa and never exceeded 3×10^{-8} Pa during evaporation. Subsequent Auger analysis showed worst case contamination level below 1.8 at% of carbon and 0.9 at% oxygen. Typically, however, the level of contamination was significantly lower (0.6 at% of C and O), but careful analysis of growth morphology and the structure of the film after the complete transformation showed no significant differences between these films. The overall contamination was, therefore, sufficiently below the level at which C and O can affect nucleation, agglomeration and transformation processes as observed by the non-atomic scale resolution STM.

Iron was deposited in small steps (less than 0.5 ML) with the sample inside a custom-designed scanning tunneling microscope (STM) [19] and

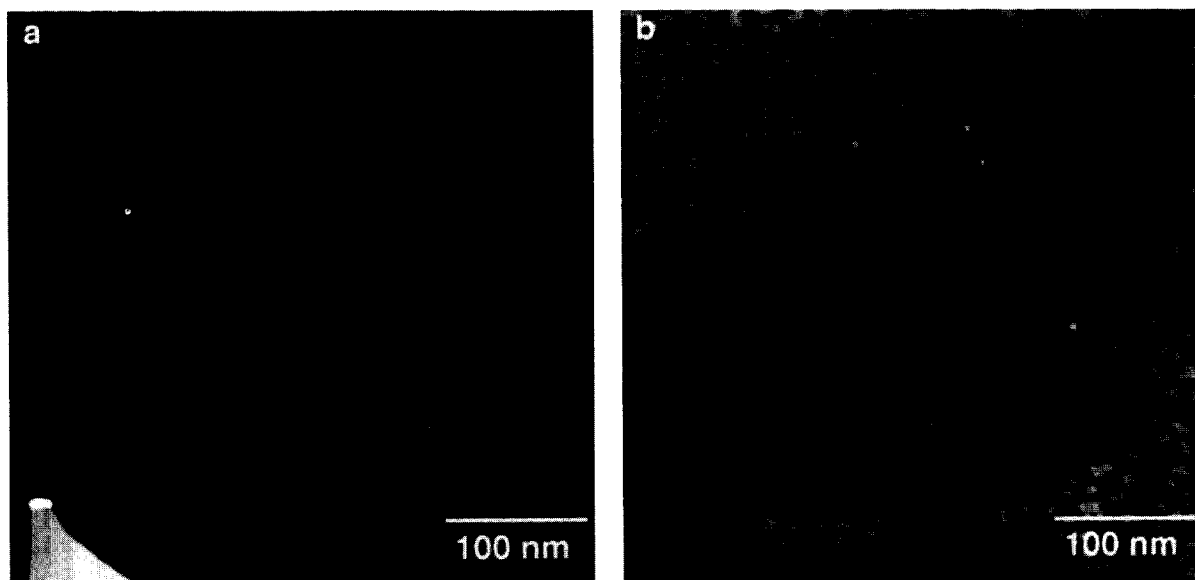


Fig. 1. (a) STM topography image from a clean Cu(100) surface and (b) 3.4 ML thick iron film grown at the same location. The area is 400×400 nm². The sample bias is 0.95 V and the tunneling current is 0.14 nA. Note a monatomic step terminating at two screw dislocations. This feature is used as a location mark in images shown later. The images are drift corrected.

the tip fully retracted by applying the maximum piezo voltage ($1 \mu\text{m}$). Coverage calibration was accomplished by imaging the surface after each evaporation step and calculating the distribution of iron in all monatomic layers. We estimate the accuracy of such calibration to be better than 0.2 ML. At no point have we seen any evidence for submonolayer step height features that were reported by others [8,16] and taken to indicate copper/iron intermixing. We observe such submonolayer features only at elevated substrate temperatures [17]. The layer distribution ratio for the nominal 1 ML coverage was quite repeatable for numerous experiments performed in this laboratory over the course of several months and is 88%, 11% and $<1\%$ for the first, second and third layer, respectively. It differs somewhat from

results reported by some other groups [16], but the origin of this difference is unclear at this point.

All images shown in this paper are constant current topography (CCT) maps. Periodic checks revealed no significant dependence of the images presented here on tunneling parameters.

3.2. Phase transformation evolution

As discussed above, iron films grown on the copper (100) surface at RT follow three distinct phases. In the first phase the growth mode is VW-like with a characteristic high nucleation density and multilayer island formation. Later on, the growth gradually switches to layer-by-layer FV-like mode with much reduced nucleation den-

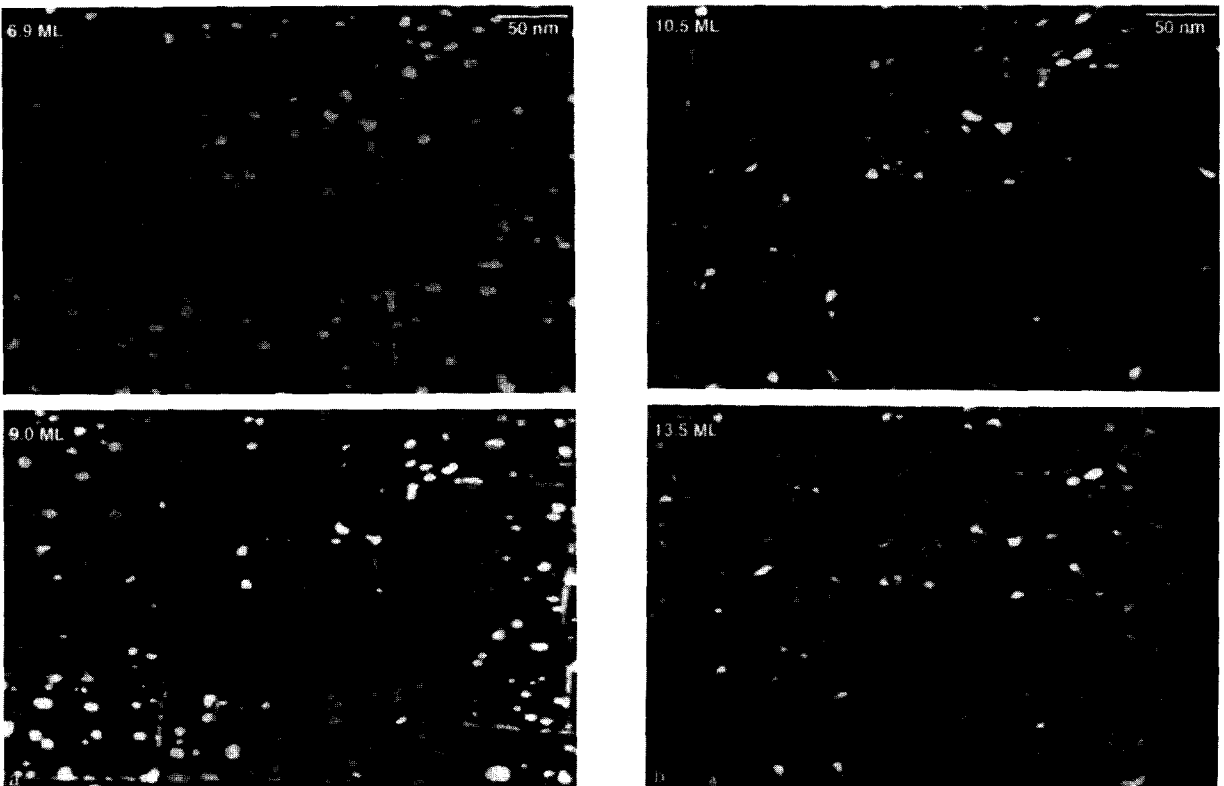


Fig. 2. (a) STM topography images of the surface area shown in Fig. 1 after incremental evaporation of iron. The scanned area is $400 \times 270 \text{ nm}^2$ and tunneling parameters are the same as in Fig. 1. All images are drift corrected. Image boundaries are parallel to the $\langle 110 \rangle$ directions of the underlying (100) fcc Cu surface to within $\pm 1^\circ$. Note the development of a weak dislocation network in the $\langle 110 \rangle$ directions into rows of flake-like features which occupy more and more of the surface area. (b) See (a).

sity. An example of the surface topography in the intermediate stage is shown in Fig. 1b. The topography of this 3.4 ML thick film shows an almost completed third layer, a large number of fourth layer islands and a small number of fifth layer nucleation sites.

An interesting feature seen in this image is the difference in the nucleation density of the fourth layer islands around the fault line. It reflects most likely an enhanced sticking probability at the step edge, but its full discussion is beyond the scope of this paper.

A series of STM images shown in Fig. 2 illustrates the evolution of the surface topography starting with the well established layer-by-layer growth mode (6.9 ML image) and ending at the 13.5 ML thick iron film, where MEED results of other groups indicate severe roughening of the surface. Note that in accordance with MEED results the 13.5 ML film surface is indeed very rough (1.5 nm peak-to-peak, and 0.23 nm rms), although some areas of undisturbed fcc phase are still seen.

However, the most surprising effect seen in this series of images is the appearance of surface restructuring well below the onset of MEED decay. For example, the 6.9 ML film (Fig. 2) already shows a well developed network of thin ridge-like lines that tend to follow the $\langle 110 \rangle_{\text{fcc}}$ close-packed directions. In fact, such features are already seen in 4.6 ML film, although at a much reduced density. To the best of our knowledge this is the first experimental indication that iron films grown at RT on the Cu(100) surface are unstable toward restructuring at coverages as low as 4.6 ML. This is the beginning of the region II discussed above where MEED results indicate an almost ideal layer-by-layer growth mode [10]. It is not surprising that this surface restructuring escaped detection in MEED and (SPA) LEED experiments because the area affected by these thin ridge-like lines is initially very small and because these probes have rather limited transverse correlation length.

It is clear from Fig. 2 that these features undergo major morphological changes as the film growth progresses. Note, however, that the original copper surface fault line still seen in all

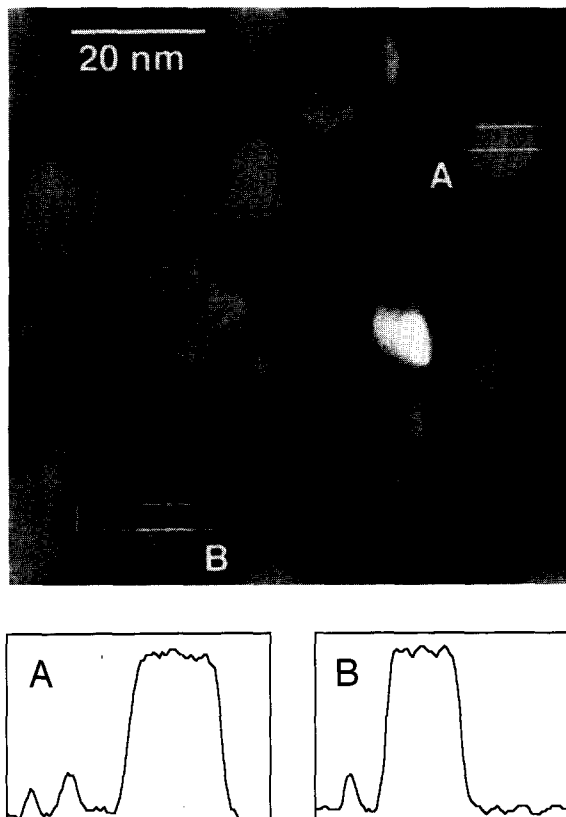


Fig. 3. Pseudo-relief STM topography image of $60 \times 60 \text{ nm}^2$ area of a 6.3 ML thick iron film on Cu(100) showing ridge-like initial transformation structures parallel to the $\langle 110 \rangle$ substrate directions. They seem to cross the island structures without interaction. Averaged line scans for two surface areas denoted A and B are shown below.

images seems to have no effect on the morphology of surface restructuring.

At the initial stages of film transformation ($> 4.5 \text{ ML}$) the restructuring appears as thin elongated ridges 2 nm wide and 20 to 50 nm long. Fig. 3 shows a typical topography of these structures. They seem to terminate at step edges, and follow the $\langle 110 \rangle$ directions. Often, they appear in groups separated by 3–5 nm width ridge lines extending in opposite directions from some nucleation site. Topographically they are buckled, symmetric features with vertical dimensions that are significantly below the fcc monolayer step height seen in the neighboring islands ($\approx 0.17 \text{ nm}$). They cross step edges without interference.

At later stages they grow wider, higher and longer. This trend can already be observed in Fig. 3. The ridge line marked B and the two thinner structures of the triplet A seen in the upper right corner of this image are ~ 0.03 nm high and ~ 2 nm wide as seen in the line plot. The third member of the triplet A (not shown in the line plot) is taller and wider. This distinct relationship between the width and the height of these features is shown in Fig. 4a.

The overall density of these features increases with film thickness and is on the order of $1.5 \times 10^{11} \text{ cm}^{-2}$ when they are first observed (4.6 ML) and $3.5 \times 10^{12} \text{ cm}^{-2}$ for 9 ML thick film. The total length jumps by almost one order of magnitude between the onset of network formation at 4.6 and 5 ML, and then gradually increases to reach a value of 0.04 nm/nm^2 at 9 ML. These findings are summarized in Fig. 4b. The length of individual lines does not change as dramatically; the maximum observed length is on the order of 300 nm. This maximum length is most likely determined by the interaction of individual transformation areas as they start crossing each other with increasing nucleation density.

Another interesting feature seen in Fig. 2 is the relative direction of these ridge-like structures. While the majority of them follow $\langle 110 \rangle$ close-packed directions of the underlying Cu(100)

surface (parallel to image boundaries), some nucleate at a slight angle ($\pm 3\text{--}4^\circ$) relative to $\langle 110 \rangle$ directions.

The origin of the ridge-like structures is difficult to determine. Wuttig et al. [18] suggested that they could be consistent with stacking faults generated by Shockley or Frank partial misfit dislocations [10]. The trend observed in Fig. 4a (height increasing with width) is not inconsistent with such a mechanism; a dislocation once nucleated may develop in ways that are hard to understand or predict a priori. However, the general question arises about the significance of any concept of dislocation classification when the core structure dimensions are on the same order of magnitude as the thickness of the surrounding material. It may be assumed in a more speculative way that the mutual complex interactions of surface and interface effects, superimposed strains and the starting stage of a transformation will affect the process of dislocation generation in such a way that only further growth will decide on the true type of a given dislocation. Thus the nucleation and the early stages of these dislocations could be considered in the context of generalized pre-defects, and may be related to the lattice instabilities and imperfections as discussed in the localized soft mode model (cf. e.g. Ref. [33]). Such a generalization in the early stages of

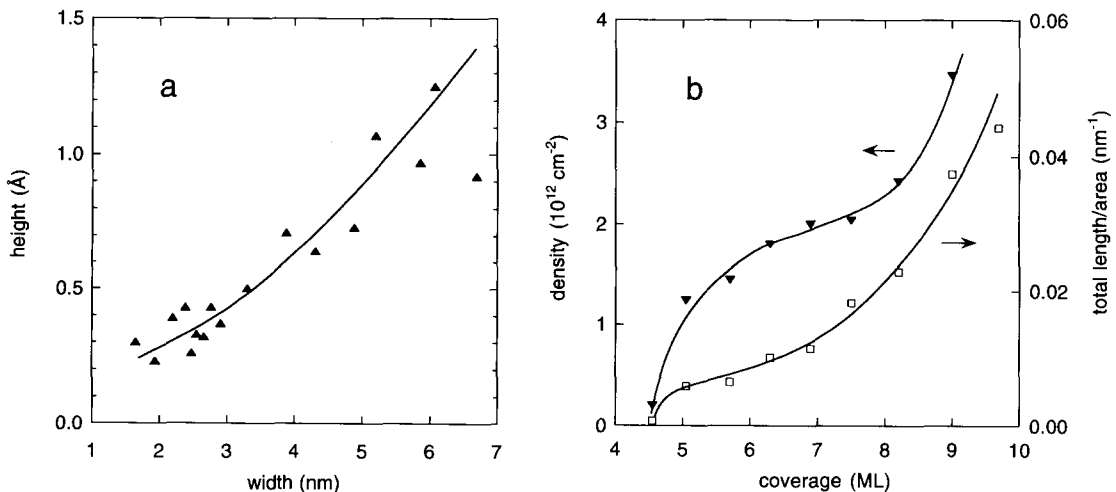


Fig. 4. (a) Correlation of width with height for ridge-like symmetric transformation line structures. (b) Dislocation line density, and total line length per area as a function of film thickness. Solid lines are only guides to the eye.

dislocation evolution seems to be supported by trends indicated by Fig. 4a. Under these restrictions we will further use the term dislocation.

The thin symmetric dislocation lines seen in the initial stages of growth change their morphology rather quickly. They become much broader and in later stages acquire a very complicated morphology – see Fig. 2b. A series of images shown in Fig. 5 demonstrates how such surface features transform. This figure follows the development of surface restructuring of a small $75 \times 75 \text{ nm}^2$ patch of the surface.

The series starts with a 6.0 ML thick film. This film is still not atomically smooth – openings to the fifth layer and the seventh layer islands are

clearly visible. The terrace step edge is seen on the left side together with an elongated transformation region bounded on both sides by the undisturbed fcc growth areas. There are two distinct features in this transformation region labeled A and B, respectively. The overall axis of this region is 3° off the $[110]$ direction. Later on, another transformation region develops. This later structure – feature C in the 9.5 ML image – seems to follow the $[\bar{1}\bar{1}0]$ direction of the underlying fcc lattice exactly. All these three features transform in different ways. We will discuss them in succession.

Feature B, as first seen in the 6.0 ML image, has the same topography as the features seen in

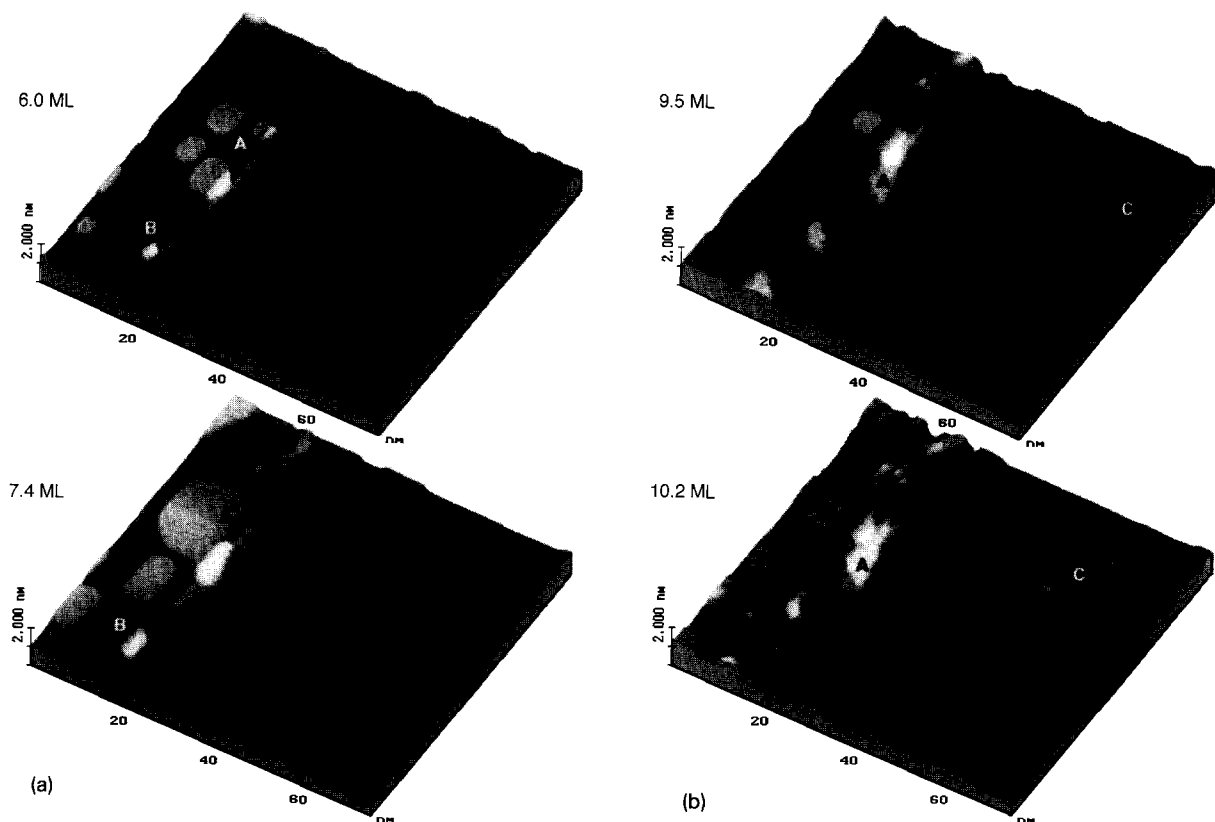


Fig. 5. (a) Series of perspective STM topography images of the same surface area after sequential deposition of iron reflecting the development of typical transformation structures on a scale smaller than in Fig. 2 ($75 \times 75 \text{ nm}^2$). The series covers the whole transformation range starting from the formation of single ridge-like features to the flake-like bcc precipitates in the later stages of film growth. (b) See caption to (a). Note the appearance of another transformation area (C) extending to the right of the original one (A,B).

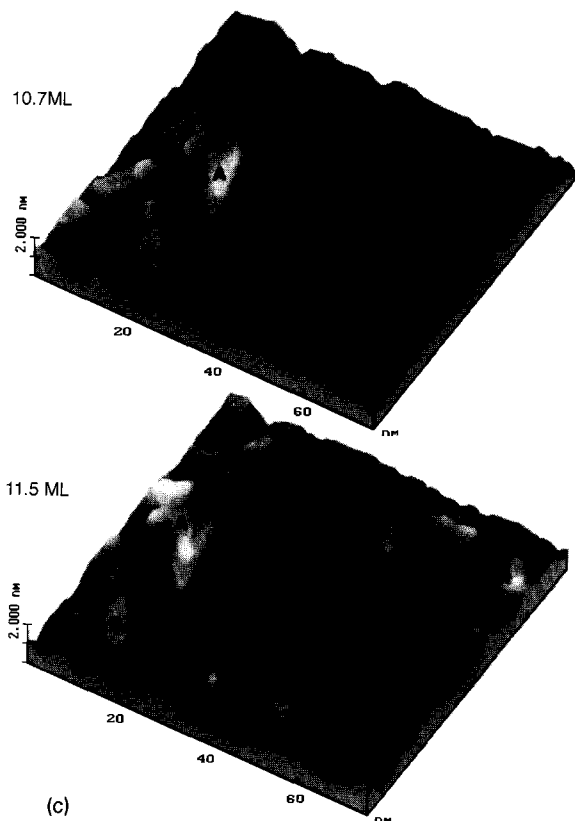


Fig. 5. (c) See caption to (a). 11.5 ML image represents a characteristic topography of almost fully transformed area.

much earlier stages of transformation; i.e. it is a symmetric buckled structure. It develops very quickly into a flat-topped parallelogram-shaped island (10.2 ML image) separated from the surrounding area by shallow grooves. The shear angle of this parallelogram is not well defined but appears to be close to $50^\circ \pm 5^\circ$. As noted in Ref. [16], the 55° angle is the angle between the [111] and [001] directions in the bcc (110) plane. Further confirmation of the bcc character of this precipitate comes from its height. Its top layer is significantly out of registry with the fcc-Fe interplanar distance strongly suggesting that the underlying structure is already a fully transformed bcc phase precipitate.

Features A and C nucleate initially in a similar way but will transform in much different ways. When first observed they are slightly tilted planes

(see Fig. 6 for a detailed view of feature C in its initial stage) that emerge smoothly from the surrounding fcc area and reach maximum heights that vary from one to several fcc-Fe interplanar distances. On the other side there is a sharp drop to a small groove whose depth is on the order of 10 to 20% of the fcc step height. The sharpness of the drop is difficult to quantify because of tip shape effects. The planes are tilted on average about 3° , have a width of 3–5 nm and seem to cross monatomic steps of neighboring islands and holes without interference. There is nothing in the morphology of these tilted structures that could indicate that they are already well formed bcc precipitates.

With increasing thickness the feature A develops a very complicated structure. On its lower side (10.2 ML image of Fig. 5b), it appears as a system of *flat* planes similar to those seen in feature B. The comparison of step heights (see Fig. 7) of this flat area with that of the neighboring undisturbed fcc growth show steps that are significantly out of registry with the fcc-Fe(100) lattice. They have an average value of 0.20 nm which is consistent with the interlayer distance of the bcc phase of iron oriented with the (110) plane parallel to the surface. Thus the lower area of the feature A is already bcc transformed. On

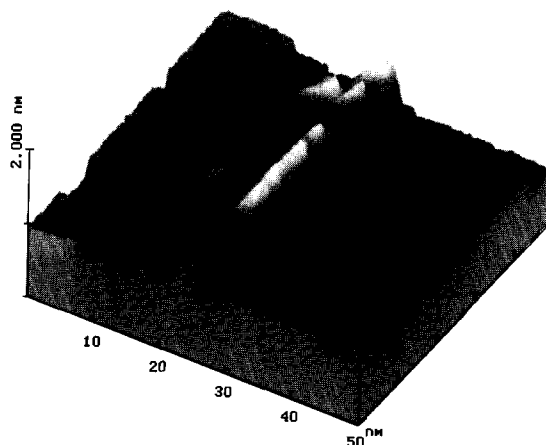


Fig. 6. STM topography image of a $50 \times 50 \text{ nm}^2$ section of feature C originally shown in 9.5 ML image of Fig. 5b. The image is rotated to show the details of a typical tilted-plane film restructuring area.

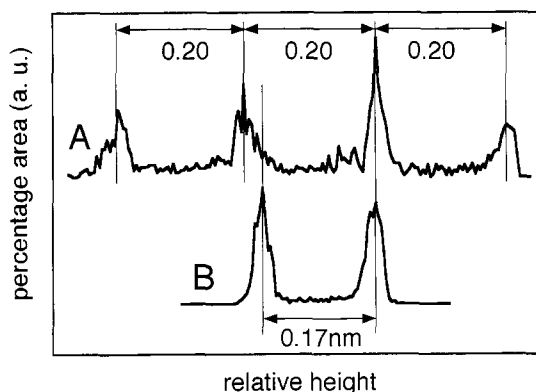
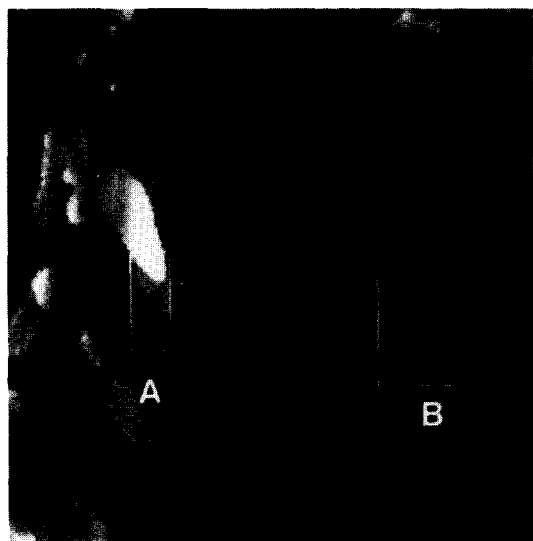


Fig. 7. Height distribution of two areas denoted A and B, and indicated by white rectangles in the STM image of 10.7 ML thick iron film shown originally in Fig. 5c. The difference in layer distance is consistent with identification of B as an untransformed fcc-Fe and A as a fully transformed bcc-Fe precipitate.

the other hand, the other (top) side of the feature A (10.2 ML image of Fig. 5b) still clearly shows the initial tilted plane system connected smoothly with the neighboring fcc area. Therefore the overall complexity of the feature A at this stage is not surprising – feature A must include some sort of an accommodation zone between its bcc and fcc parts.

The lower bcc side of the structure A is separated from the surrounding area by a groove

system similar to the one seen around feature B. This groove system seems to follow the morphology: it exists only around flat plane systems; the tilted plane system is still smoothly connected with the neighboring, untransformed fcc area. Thus it appears that in order to form a homogeneous bcc precipitate the connection to the surrounding fcc area must be weakened. Such a weakening is most likely provided by a groove seen around these features. The tip shape effects preclude precise determination of their depth, but they appear to be no deeper than one fcc-Fe plane. With further deposition (10.7 and 11.5 ML images) the morphology of this area becomes too complex for any simple interpretation.

Still another type of transformation behavior is seen in the feature C (9.5 ML image). This feature develops in a much different way than the feature A despite the fact that they originally nucleated in a similar form. However, their similarity at the nucleation point is not exact. C is initially slightly more complicated as seen in the magnified (and rotated to better show the structure) image shown in Fig. 6. Its smaller lower part consists of two tilted planes with step heights of nearly one and two fcc interplanar distances whereas its major part appears as a single tilted plane terminating in a three layer high fcc step. An additional exposure of only 0.7 ML results in an extensive system of similarly tilted planes (Fig. 5, 10.2 ML image) with the step heights still commensurate with the fcc lattice.

With a deposition of another 0.5 ML a complete restructuring of the upper fcc area leads to the formation of a symmetric feature surrounded on both sides by oppositely tilted planes (10.7 ML). This feature is shown in more detail in Fig. 8. Note the island in the top layer which is flat in one direction and bent in the other. It has a relatively flat middle part which is parallel to the Cu(100) surface but its borders are bent to fit the inclination of the surrounding area. The step heights of the three uppermost layers are clearly out of registry with the fcc lattice and seem to fit the bcc (110) interplanar spacing. Thus this feature appears as another kind of bcc precipitate. The bending of its top layer most likely reflects an accommodation zone between the central part

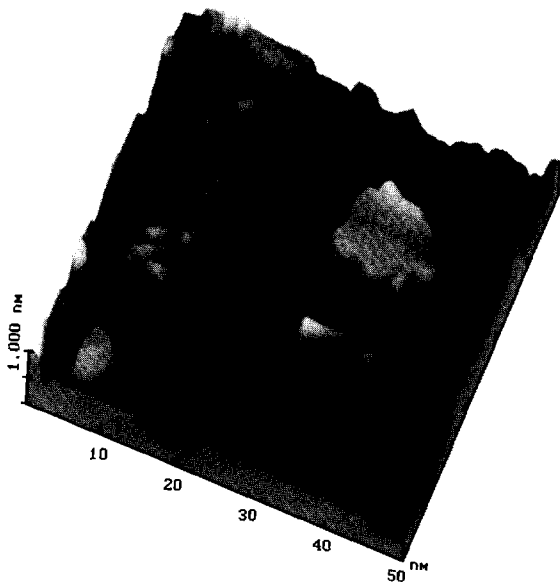


Fig. 8. Perspective STM topography image of $50 \times 50 \text{ nm}^2$ zoomed area of the 10.7 ML thick iron film in Fig. 5c showing in detail a symmetric feature terminated by multi-step systems with oppositely tilted planes. Note the island-shaped feature in the top layer which is flat in one direction and bent in the other. This bending most likely represents an accommodation zone between the central part and the surrounding tilted plane systems.

and the surrounding tilted plane systems. Further deposition does not change the overall morphology of this system indicating its relative stability – see Fig. 5, 11.5 ML image.

In the final stages of transformation most of the surface area shows severe restructuring with a rich variety of structures. One characteristic feature, however, is a system of mutually oriented grains. A small area of surface shown in Fig. 5c (10.7 ML image) shows already this characteristic orientation; see for example a structure mirroring feature B across the transformation area axis in the 10.7 ML image. On larger scale (13.5 ML image in Fig. 2) they appear as long parallel chains of parallelogram-like flakes that seem to be sheared symmetrically to the chain direction. They are quite similar in appearance to those reported by Chambliss et al. [16]. Such a grain system can indicate twinning induced by a martensitic shear transformation.

4. Discussion

The picture that emerges from the summary of the experimental findings given above is that of an extremely complicated transformation behavior. It is beyond the scope of this paper to attempt to describe and explain all the features of the transformation reported above. Instead we will limit ourselves to a discussion of all the factors that can influence this transformation and make reference to the experimental findings whenever the connection to the theory can be clearly established. Our primary goal here is to set the stage for further work in this area.

Any attempt to properly interpret the STM observations reported above should proceed from careful consideration of all factors involved including pseudomorphic growth, misfit accommodation and interface structures that are specific to thin film system. It should also properly take into account the peculiarities of this experimental system: namely the fact that we are observing restructuring processes induced by changing thickness in a system that is unstable toward a major structural phase transformation and the fact that growth itself can change the film morphology to a significant degree. In this discussion we will also try to make contact with previous findings concerning transformation paths and the geometry of lattice rearrangements in bulk iron and in thicker iron film systems.

The estimation of the critical layer thickness for the formation of misfit dislocations depends on the mechanism responsible for their generation, i.e. gliding of existing substrate dislocations via a force balance within the strained epitaxial system (which in our case of nearly dislocation free surfaces is not valid) or spontaneous generation to reduce the strain energy of the film (cf. e.g. Refs. [27,34,35]). In the case of complete pseudomorphism (film is strained to a perfect fit) the approximation for the first type predicts $d_c = 5.5 \text{ nm}$ (equivalent to 30 ML thick fcc-Fe film), and other models yield nearly 4 and 6 nm (21 and 33 ML, respectively) [29].

Of course, such calculations are rough approximations for several reasons. The interface models appropriate to consider for the spontaneous

generation of misfit dislocations are theories of equilibrium and, therefore, describe only the most favorable final configuration without involving growth kinetics and interaction of lattice imperfections. Moreover, many essential parameters are either unknown or not known with sufficient accuracy, e.g. the strength of interface interactions, the specific surface state of the substrate and mechanical parameters of the interface [35].

The occurrence of misfit dislocations at lower film thicknesses than predicted by those theories should not, therefore, be particularly surprising. In addition, the generation of defects in this system will be influenced by strains, which are not only due to misfits but also due to the initial stages of transformation. Both sources of strain interact and influence each other. Such interactions will be enhanced by the fact that neighboring areas could be in different stages of transformation.

Once the dislocations occur, the interface will become semicoherent and the dislocations will act as nucleation sites for further transformation. Such a process is well known to control the formation and growth of a product phase in martensitic transformations (for problems of martensitic nucleation see e.g. Refs. [33,36,37]).

The existence of misfit dislocations in the Fe/Cu thin film system prior to the transformation process corresponds with the observations on γ -Fe precipitates in a Cu–1.95wt%Fe alloy [38]. The precipitates are elastically strained up to nearly 60 nm in diameter to accommodate the misfit. No faults, grain boundaries or dislocations are seen below this size. Exceeding this diameter, the precipitates become semicoherent, i.e. they are surrounded by interface dislocations. Long after the appearance of these dislocations a transformation into the bcc structure was observed, i.e. the γ -Fe precipitates in fcc Cu must become semicoherent before the new phase is formed, as is the γ -Fe layer on copper system in our case.

As a consequence of nucleation and growth of bcc precipitates within the fcc matrix the misfit can locally increase from -1.1% to almost -10% and the film can, therefore, be subdivided and dissected to assume a flake-like shape. Such re-

structuring could occur to reduce the overall transformation strain. Possibly the observed decomposition of the layer in final stages (cf. Fig. 5c, 11.5 ML image) indicates this process. In an analogous manner the overall strain in bulk samples is reduced by lattice invariant shear deformations that lead to twinned or slipped regions which in turn are reflected in a characteristic martensitic surface relief.

The special orientation relation occurring between a bcc precipitate and the surrounding fcc matrix depends strongly on the applied stress, i.e. on the crystallographical misfits. The stress is also expected to be influenced by island shapes and interface defects. To investigate the way in which a given stress state will control the transformation one can compare the growth mode of the Fe–Cu and the Fe–Ni systems. The absolute value of the misfit is quite similar in these systems (around 1.2%) but they have opposite signs: iron is under tensile stress on the copper substrate while it is in compressive stress on the nickel. In the Fe–Ni system [39] the bcc iron precipitates occur in four of the twelve variants of an orientation relationship described by Pitsch [40]. In the Fe–Cu system, the early TEM work [30,31] showed also the predominance of the Pitsch orientation relationship; however, the variants were different from those observed in the Fe–Ni system. The special orientations observed in the Fe–Cu system are absent in the Fe–Ni system and vice versa. Such asymmetry clearly reflects the influence of the applied strain on details of the transformation geometry.

The reason for the preference of *Pitsch* variants in a given thin film system is that the largest principal axis of transformation strain of the resulting bcc phase is perpendicular to the film plane and that the corresponding relatively large changes in lattice constants can be tolerated best in *thin* films.

A Pitsch orientation relationship between fcc and bcc phases is present if $\{100\}_{\text{fcc}}$ is parallel to $(\bar{1}10)_{\text{bcc}}$ and $\langle 110 \rangle_{\text{fcc}}$ is parallel to $[112]_{\text{bcc}}$. The combination of these planes and directions represents the possible twelve variants of Pitsch relationships.

It is difficult to predict whether a given path of

transformation will occur or not and in which variant, as it strongly depends on the actual stress state. A semi-quantitative analysis of the effective interaction energy density and the driving force for the formation of the bcc precipitate [32] yields some insight into the dependence of the transformation on orientation and misfit strain. Generally, the observed precipitate orientation relationships in iron films [32] indeed were those having the most negative interaction energy density and whose shear mechanisms are aided by the misfit stress. The atomic movement during transformation into a bcc region of given orientation follows a specific path which is influenced by the applied stress. The corresponding shear mechanisms involve particular shear systems onto which the applied stress is resolved. A possible shear mechanism for the Pitsch relationship is the shear system consisting of a $\{110\}$ shear plane and a $\langle\bar{1}\bar{1}0\rangle$ shear direction. The corresponding shear angle is $19^{\circ}28'$.

Our STM observations of ultrathin films grown under UHV also seem to give an indication for the activation of this particular shear mechanism. That includes the characteristic $\langle\bar{1}\bar{1}0\rangle$ direction of the ridge pattern seen in Fig. 2 and the inclination of neighboring regions observed in the tilted plane region (Fig. 6). These may as well be the initiating steps of such rearrangement processes. The alternative Kurdjumov–Sachs or Nishiyama orientation relationships would involve shear systems with either a $\{\bar{2}11\}$ shear plane or a shear in the $\langle\bar{2}11\rangle$ direction for which we could not find any direct evidence at this stage of investigation.

A more precise determination of the orientation of observable structural features is currently under investigation and will be published in a forthcoming paper.

A further insight into the complex phenomena forming the background of our observations is expected by lattice dynamic calculations taking into account the interference of thin film growth, lattice accommodation and phase transformation.

5. Conclusions

It is an unexpected disadvantage of the fcc-Fe/Cu(100) system which initially seemed so

promising as a candidate for a novel 2D magnetic system that it turned out to be structurally much more complex than originally assumed. On the other hand, the unexpected richness of this system provides ample opportunity to study basic processes of film growth. The iron/copper ultrathin film system is especially interesting because its inherent thermodynamic instability has such a pronounced effect on morphology and structure of these films. The film system shows features similar to those observed and studied in bulk materials for a long time but at the same time differs sufficiently enough to provide new insights into mechanisms and driving forces of these transitions – especially into the first steps of martensitic transformations.

The original confusion regarding initial stages of growth is still not fully resolved and the drastic roughening of the thicker films (region III) is now well established. Furthermore, as reported here, even in the thickness region where the system was previously seen as well behaved, the inherent instability toward the bcc transformation manifest itself quite visibly in real space (CCT) images. “It is hard to escape the physical fact that the fcc-Fe on Cu(100) is in a high-energy configuration” as succinctly pointed out by authors of Ref. [16].

The work reported here follows this transformation in detail. The original “nucleation sites” were identified at coverages as low as 4.6 ML. Their nature at this point is controversial; they could be interpreted as dislocation lines, but such a concept is not well established or understood due to the fact that the core dimensions of dislocations in fcc metals are of the same order of magnitude as this film thickness. (A complete edge dislocation in copper was calculated to have a width of about five Burgers vectors (1.3 nm) and the linear elasticity theory breaks down inside a core radius of 0.9 nm [41].)

At least three distinct types of behavior have been identified in the evolution of the initial transformation areas. At this point it appears that the Pitsch orientation relationship is a predominant one in these structures. The large number of the observed types of transformation behavior simply reflects the complexity of processes that drive this transformation and their mutual inter-

actions. We enumerated all those processes but a fuller understanding must come from further theoretical work.

The occurrence of dislocations at 4.6 ML appears to be consistent with the recent state-of-the-art *IV*-LEED structural analysis of Wuttig and Heinz [42]. According to their calculations, the 4 ML thick iron film is strained to a perfect fit with the copper substrate while the slightly thicker films (6–8 ML) show significant relaxation of the top-most layers with iron assuming its expected fcc in-plane lattice constant. It is very likely that such a relaxation is made possible by the formation of the stress relieving dislocation network that we observe at 4.6 ML. Similar 4–5 ML structural discontinuity has been also reported in much older LEED work by Clarke et al. [43]. It is now clear that the three regions of iron growth on Cu(100) as classified by Wuttig et al. [10] reflect the inherent structural instability of this system. In region I, the film is completely pseudomorphic with the underlying copper substrate, while in region II the film is still predominantly fcc-like but an extensive network of dislocations is generated to accommodate the growing stress. And, as previously reported, region III is dominated by bcc grains whose size and distribution reflect the large mismatch of this iron phase with the copper substrate.

An interesting question regards the extent to which such a structural rearrangement can affect magnetic properties of these films, and, in fact, whether magnetism itself plays any role in the transformation. While the definite answer must await further investigation, the existing data seem to imply that such a correlation does, indeed, exist. Thomassen et al. [6] report a major change in the magnetization properties of the room-temperature grown fcc-Fe/Cu(100) film around 4–5 ML. Below 4 ML the film is uniformly magnetized, whereas above 5 ML the magnetization is confined to surface layer (the so-called magnetic live surface layer). Later, the film switches from perpendicular to in-plane magnetization at ~11 ML i.e. where the bcc phase is a dominant one in the film. For Fe films grown at low temperatures (90 K) the behavior is different. Allenspach et al. [44] found that these fcc-Fe/Cu(100) films un-

dergo a transition from perpendicular to in-plane magnetization at the thickness of ~5 ML. The strong correlation of magnetic behavior reported by Thomassen et al. with our findings (i.e. with the onset of the dislocation network at 4.6 ML) suggests that the structural instabilities of this system have a major effect on its magnetism. It remains to be seen [17] if the 4–5 ML critical thickness reported by Allenspach et al. [44] for cold-evaporated films is connected with a similar structural rearrangement.

Acknowledgment

This work was supported by the Deutsche Forschungsgemeinschaft through Sonderforschungsbereich 6.

References

- [1] CRC Handbook of Chemistry and Physics (CRC Press, Boca Raton, FL, 1993).
- [2] There is some indication that fcc-Fe exists in two forms differing in volume and magnetic properties – see for example: O.K. Andersen et al., *Physica B* 86–88 (1977) 249; G.L. Krasko and G.B. Olson, *Phys. Rev. B* 40 (1989) 11536.
- [3] C.S. Wang, B.M. Klein and H. Krakauer, *Phys. Rev. Lett.* 54 (1985) 1852.
- [4] F.J. Pinski, J. Stautontont, B.L. Gyorffy, D.D. Johnson and G.M. Stocks, *Phys. Rev. Lett.* 56 (1986) 2096.
- [5] V.L. Moruzzi, P.M. Markus, K. Schwarz and P. Mohn, *Phys. Rev. B* 34 (1986) 1784.
- [6] J. Thomassen, F. May, B. Feldmann, M. Wuttig and H. Ibach, *Phys. Rev. Lett.* 69 (1992) 3831.
- [7] D.P. Pappas, K.P. Kämper and H. Hopster, *Phys. Rev. Lett.* 64 (1990) 3179.
- [8] D.D. Chambliss, R.J. Wilson and S. Chiang, *J. Vac. Sci. Technol.* 4 (1992) 1993.
- [9] M.K. Kief and W.F. Egelhoff, Jr., *Phys. Rev. B* 47 (1993) 10785.
- [10] M. Wuttig and J. Thomassen, *Surf. Sci.* 282 (1992) 237.
- [11] T. Detzel and N. Memmel, *Surf. Sci.* 293 (1993) 227.
- [12] J. Thomassen, B. Feldmann and M. Wuttig, *Surf. Sci.* 264 (1992) 406.
- [13] D.A. Steigerwal and W.F. Egelhoff, Jr., *Surf. Sci.* 192 (1987) L887.
- [14] M. Arnot, E.M. McCash and W. Allison, *Surf. Sci.* 269/270 (1992) 724.
- [15] P. Dastoor, M. Arnot, E.M. McCash and W. Allison, *Surf. Sci.* 272 (1992) 154.

- [16] D.D. Chambliss, K. Johnson, K. Kalki, S. Chiang and R. Wilson, in: *Multilayers and Surfaces; Interfaces and Characterization*, MRS Symposia Proceedings No. 313 (Materials Research Society, Pittsburgh, 1993) p. 713; K. Kalki, D.D. Chambliss, K.E. Johnson, R.J. Wilson and S. Chiang, *Phys. Rev. B* 48 (1993), to be published.
- [17] Work in progress by the same authors; to be published later.
- [18] M. Wuttig, B. Feldmann, J. Thomassen, F. May, H. Zillgen, A. Brodde, H. Hannemann and H. Neddermeyer, *Surf. Sci.* 291 (1993) 14.
- [19] A.K. Schmid and J. Kirschner, *J. Vac. Sci. Technol. B* 9 (1991) 649.
- [20] M.T. Kief and W.F. Egelhoff, Jr., *J. Vac. Sci. Technol. A* 11 (1993) 1661.
- [21] G.A. Prinz, *J. Magn. Magn. Mater.* 100 (1991) 469.
- [22] K.S. Cheung and R.J. Harrison, *J. Appl. Phys.* 71 (1992) 4009.
- [23] M.J. Bibby and J. Gordon Parr, *J. Iron Steel Inst.* 202 (1964) 100.
- [24] Widmannstätten ferrite occurs during $\gamma \rightarrow \alpha$ transformation in coarse-grained austenite regions at higher cooling rates. The growth of the ferrite needles or platelets starts at the austenite grain boundary and the structures formed have preferred orientation, analogous to the Widmannstätten precipitates in meteoritic Fe/Ni alloys.
- [25] J.D. Watson and P.G. McDougall, *Acta Metall.* 21 (1973) 961.
- [26] H. Schumann, *Crystal Geometry: Theory of Lattice Transformations* (DVG, Leipzig, 1980).
- [27] J.H. van der Merwe, J. Woltersdorf and W.A. Jesser, *Mater. Sci. Eng.* (1986) 1.
- [28] M.J. Bilby and J.W. Christian, *J. Iron Steel Inst.* 197 (1961) 122.
- [29] W.A. Jesser and J.W. Matthews, *Philos. Mag.* 15 (1967) 1097.
- [30] W.A. Jesser and J.W. Matthews, *Philos. Mag.* 17 (1967) 595.
- [31] G.H. Olsen and W.A. Jesser, *Acta Metall.* 19 (1971) 1009.
- [32] G.H. Olsen and W.A. Jesser, *Acta Metall.* 19 (1971) 1299.
- [33] G. Guenin and P.F. Gobin, *Proc. Int. Conf. Martens. Transf. ICOMAT 79* (1979) 532.
- [34] J.W. Matthews, in: *Epitaxial Growth*, part B (Academic Press, New York, 1975) p. 560.
- [35] J. Woltersdorf, *Thin Solid Films* 85 (1981) 241.
- [36] G.B. Olson and M. Cohen, *J. Phys. C* 4–43 (1982) 75.
- [37] T. Suzuki and M. Wuttig, *Acta Metall.* 23 (1975) 1069.
- [38] K.E. Easterling and H.M. Miekko-Oja, *Acta Metall.* 15 (1967) 1133.
- [39] J.W. Matthews and W.A. Jesser, *Philos. Mag.* 20 (1969) 999.
- [40] W. Pitsch, *Philos. Mag.* 4 (1959) 477.
- [41] R.M.J. Cotterill and M. Doyama, *Phys. Rev.* 145 (1966) 465.
- [42] M. Wuttig and K. Heinz, unpublished presentation at the 3rd European Science Foundation Workshop on: "Alloy surfaces and thin metallic films" (Le Sappey en Chaux, 1993)
- [43] A. Clarke, P.J. Rous, A. Arnott, G. Jennings and R.F. Willis, *Surf. Sci.* 192 (1987) L843.
- [44] R. Allenspach and A. Bischof, *Phys. Rev. Lett.* 69 (1992) 3385.